Nanoscale Advances

ROYAL SOCIETY OF CHEMISTRY

PAPER

View Article Online
View Journal | View Issue

Cite this: *Nanoscale Adv.*, 2022, **4**, 4402

Mapping the relationship between total and functional antibodies conjugated to nanoparticles with spectrally-resolved direct stochastic optical reconstruction microscopy (SR-dSTORM)†

Emmanouil Archontakis,‡[a] Laura Woythe, ‡[a] Bas van Hoof[b] and Lorenzo Albertazzi *[ac]

Antibody-functionalized nanoparticles (NPs) have shown numerous benefits in drug delivery and biosensing, improving the specificity of cell targeting and analyte detection, respectively. However, one of the main challenges is the lack of control over antibody orientation on the NP surface. Popular and easy conjugation strategies, such as carbodiimide-based conjugations, lead to a random orientation of antibodies on the NPs, compromising ligand functionality and contributing to undesired biological effects and reduced target recognition. While new methods for more controlled NP functionalization have been proposed, there is a lack of techniques that can elucidate the orientation of the antibodies at the single-particle level to determine the conjugation outcome and, therefore, the NPs' potential in selective targeting. Here, spectrally-resolved direct stochastic optical reconstruction microscopy (SR-dSTORM), an optical super-resolution technique, is introduced to quantify the relationship between total and functional NP conjugated cetuximab antibodies at the single-particle level. An evident single-particle heterogeneity in total and functional cetuximab is observed, leading to particles with different functional : total ratios. Additionally, the results indicate that the functional : total ratio of cetuximab highly depends on the conjugated cetuximab concentration. Overall, SR-dSTORM represents a direct approach for the NP structure–functionality relationship quantification, providing a platform to improve antibody-conjugated NPs characterization and facilitating their rational design.

Received 5th July 2022
Accepted 7th September 2022

DOI: 10.1039/d2na00435f

rsc.li/nanoscale-advances

Introduction

NPs are used as drug delivery platforms to transport therapeutics to the cells of interest.[1] The NP surface can be functionalized with targeting ligands such as antibodies, peptides, or aptamers to stimulate selective recognition of a cell type.[2] However, the clinical translation of ligand-conjugated NPs is challenging, resulting in no clinically approved targeted nanotherapeutic to date. One of the pitfalls in clinical approval of ligand-conjugated control is the lack of standard and robust characterization methods to understand NP functionality at a molecular level. There is a clear need for new characterization techniques to elucidate the structure-targeting properties of ligand-conjugated NPs to understand and improve their clinical efficacy.[3]

Antibodies are commonly used NP ligands because they present two fragment antigen-binding (Fab) regions that enable strong interactions with their target.[4,5] For selective NP targeting, it is desired that the maximum number of Fab fragments are exposed after conjugation to recognize the target receptor. However, antibodies also present a fragment crystallizable (Fc) domain that does not recognize the target but can interact with receptors on immune system cells and induce the premature clearance of the NP from the body.[6] Thus, the complex interplay between Fab and Fc exposure on the NP surface can lead to unpredictable biological outcomes. Nevertheless, established procedures for NP conjugation, such as carbodiimide-based conjugation, can cause the random orientation of antibodies on the NP surface, causing a significant part of Fab fragments to be obscured and thus not able to recognize the target.[7] This substantial functionality loss is often overlooked by standard ligand characterization techniques, such as a supernatant assay, that are based on indirect measurements of NP ligands and don't provide molecular information.[8] Consequently, the

[a]*Department of Biomedical Engineering, Institute for Complex Molecular Systems (ICMS), Eindhoven University of Technology, P.O. Box 513, 5600 MB, Eindhoven, The Netherlands. E-mail: l.albertazzi@tue.nl*

[b]*Department of Applied Physics, Institute for Complex Molecular Systems, Eindhoven University of Technology, P.O. Box 513, 5600 MB, Eindhoven, The Netherlands*

[c]*Nanoscopy for Nanomedicine, Institute for Bioengineering of Catalonia, Barcelona, Spain*

† Electronic supplementary information (ESI) available. See https://doi.org/10.1039/d2na00435f

‡ These authors contributed equally.

total amount of conjugated antibodies is not representative of the functional amount, leading to a misunderstanding of the actual NP's valency and consequent targeting properties. Furthermore, recent reports indicate substantial heterogeneity in NP conjugation at a single-particle level.[9–11] Understanding NP ligand orientation and their functional heterogeneity are fundamental to achieving efficient active targeting.

This study aims to zoom into the antibody conjugation process particle-by-particle and understand which fraction of total molecules conjugated are functional over the total amount of antibodies. Techniques with molecular resolution and multiplexing capability are needed to solve this question. Transmission electron microscopy is a powerful tool to illuminate NP functionality at a single-particle level with high spatial resolution.[12,13] However, it lacks selective labelling and multicolor imaging, necessary to visualize both active and inactive antibodies. Single-molecule localization microscopy (SMLM) was recently described as a powerful tool in nanomedicine research.[14] SMLM has an improved resolution compared to standard fluorescence microscopy techniques (5–25 nm) by overcoming the optical diffraction limit and is thus able to resolve and quantify molecular details of nanostructures. Recently a functional direct stochastic optical reconstruction microscopy (dSTORM) method was developed in our lab to quantify the number of functional antibodies conjugated to NPs.[11] dSTORM is a SMLM modality that relies on the temporal separation of photoswitchable fluorophores to detect fluorescent species with high precision. Unfortunately, the multicolor quantification of dSTORM images is very challenging, as it requires two spectrally separated fluorophores with optimal photophysical properties. This is not trivial as dyes are usually best-performing in a narrow range of wavelengths in the red emission window (650–700 nm), making it challenging to distinguish these between each other. Consequently, previous work focused only on the quantification of functional antibody-conjugated nanoparticles, while the relation between total and functional molecules remained to be elucidated at a single-particle level.[11] Recently, multicolor approaches based solely on infrared dyes have been proposed, such as spectral demixing and imaging.[15]

Spectral SMLM (sSMLM) configurations enable simultaneous optical super-resolution microscopy and spectroscopy at the single-molecule level.[16] Briefly, sSMLM methods use a spectrally-dispersive optical element to provide the spatial and spectral information of single molecules simultaneously. This innovative method was first implemented for functional super-resolution microscopy using Points Accumulation for Imaging in Nanoscale Topography (PAINT) as a SMLM tool combined with environmentally sensitive fluorophores such as Nile Red.[16–18] Additionally, sSMLM has been described for multicolor super-resolution microscopy of cellular structures using either STORM or PAINT.[15,18–20]

Herein, spectrally-resolved dSTORM (SR-dSTORM) is introduced as a tool to quantify the total *versus* functional cetuximab antibodies conjugated to silica NPs simultaneously. Therefore, a double-labeling strategy has been devised to stain the total and the functional cetuximab fractions separately, giving insight into the NPs' targeting properties. The multiplexing imaging capability of SR-dSTORM enabled the discrimination of red-emitting dSTORM fluorophores with emission peaks only tens of nanometer apart. First, the therapeutic antibody cetuximab was labelled prior to NP conjugation to mark the total number of conjugated antibodies. Then, a labelled Fab-specific probe was used to detect the functional sites post NP functionalization. The resulting SR-dSTORM image mapped each NP in two colors: one representative of the number of total cetuximab and the second defining the functional cetuximab Fabs. The single-molecule spectral resolution of the technique enabled the quantification of single-particle heterogeneities, illuminating the differences in cetuximab total amount, functional amount, and the functional : total ratio between NPs of the same batch. Notably, differences in the functionality of cetuximab-conjugated NPs were observed when the cetuximab concentration was varied. The functional : total ratio per NP did not remain constant, with lower ratios at higher cetuximab conjugation concentrations.

The presented SR-dSTORM method enabled the first quantification of functional and total antibodies at the single-particle level, paving the way towards the use of spectrally-resolved single-molecule microscopy to understand ligand orientation after NP conjugation. In this context, multicolor NP mapping can improve the fundamental understanding of NP structure and functionality, potentially predicting the implications of these two properties on cell targeting. Furthermore, the presented method can be expanded to additional research areas were ligand functionality is indispensable, such as the characterization of antibody-coated nanoparticles for biosensing applications.

Results and discussion

In order to understand the antibody orientation on the NP surface, a SR-dSTORM workflow was performed to quantify the amount of total and functional cetuximab Fab fragments on single NPs (Fig. 1). First, to quantify the total amount of cetuximab, the antibody was labelled with CF680 before being conjugated *via* carbodiimide (EDC)-based chemistry to NPs (Fig. 1A). Subsequently, the functional amount of antibodies were tagged using an AF647-labelled recombinant EGFR probe that binds to the exposed Fab fragments of the cetuximab antibody, as previously described.[11] Finally, both molecules were imaged simultaneously using SR-dSTORM, and their respective signals were distinguished based on the single-molecule fluorescence spectrum, creating multiplexed single-particle localization maps of total and functional antibodies. This was achieved by placing a diffraction grating in front of the camera in order to separate the spatial (0^{th} diffraction order) and spectral (1^{st} diffraction order) profiles into two different regions (Fig. 1B). This allowed the quantification of the amount of localizations based on the spectral fingerprints of each single dSTORM localization. Since the amount of dSTORM localizations is proportional to the amount of total or functional molecules, it is possible to quantify antibody amount and functionality on a single-particle basis and extract information

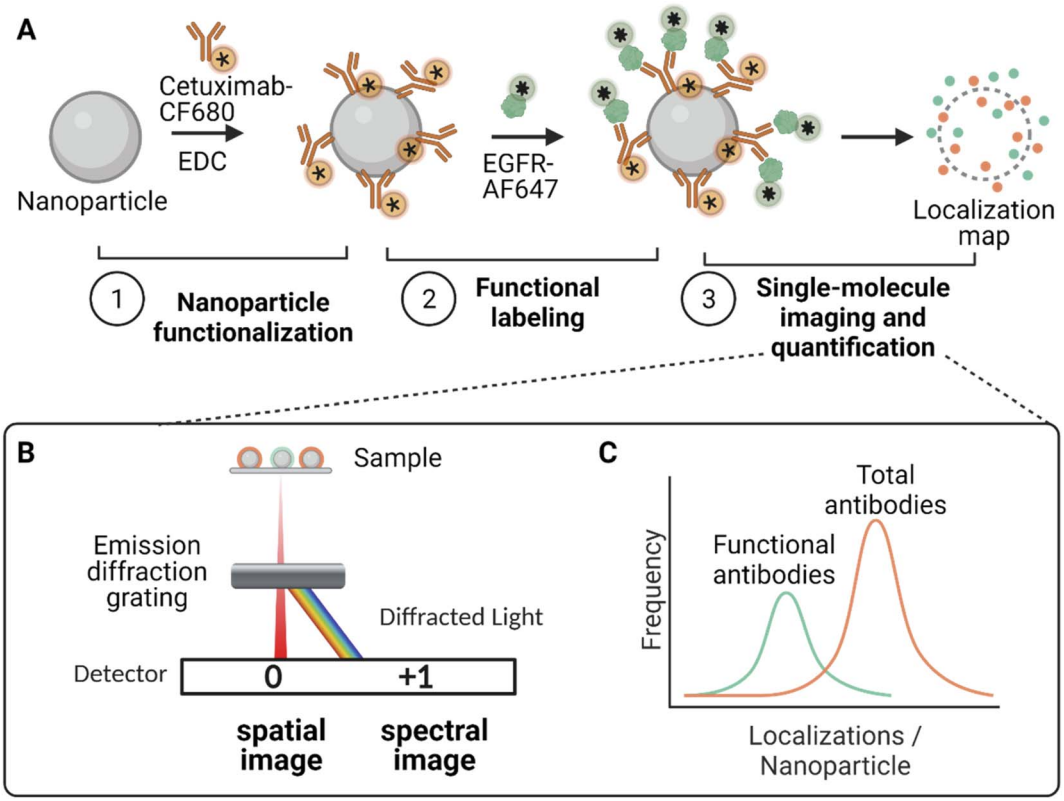

Fig. 1 Schematic representation of SR-dSTORM for quantifying the total and functional amount of antibodies. (A) Silica NPs were functionalized with CF680-labelled cetuximab antibodies using carbodiimide (EDC) chemistry. Next, functional antibody sites were labelled using AF647-labelled EGFR probe. Finally, total and functionalized antibodies were imaged and quantified. (B) SR-dSTORM was performed by using a diffraction grating that separates the fluorescence signal originating from the sample into two regions; the 0^{th} order of diffraction representing the spatial domain and the 1^{st} order of diffraction the spectral domain. (C) Single-molecule localizations were detected to quantify the fraction of functional and total antibodies at a single-particle level.

about the heterogeneity of the functionality in the NP formulation (Fig. 1C).

Fig. 2 presents a typical SR-dSTORM readout from cetuximab/EGFR-functionalized NPs. The addition of an optical grating in front of the camera separates the field of view, through diffraction, into a spatial region (Fig. 2A left), in which the position of the fluorophore is localized, and a spectral region (Fig. 2A right), which consist of a dispersed point containing information about the emission and identity of the fluorophore. The spatial to spectral pixel distance was calibrated according to the fluorophore's emission spectrum (665 nm for AF647 and 698 nm for CF680, respectively) to extract the pixel-to-wavelength ratio (ESI Fig. S1†). An example of the raw single-molecule spectra from a selected NP is represented in Fig. 2B. Each green line spectrum corresponds to an AF647 localization, while each orange line spectrum corresponds to a CF680 localization. All spectra peaks appeared very well spectrally-resolved (~30 nm) and matched the actual wavelength peaks of the two fluorophores.

An overview of a representative field of view showing the multiplexing dSTORM image is displayed in Fig. 2C. Each NP has a finite amount of molecules (AF647 and CF680) which appear with three main pseudocolors (red, green, blue), while white is generated due to their superposition. These results demonstrate that a two-color multiplexing imaging of antibody-functionalized silica NPs to probe the total *versus* functional antibodies simultaneously is possible with SR-dSTORM. These results can be quantified, estimating the average functional properties using the localizations at the single-particle level (Fig. 2D). Specifically, by fitting a Gaussian profile each spectrum, each molecule was assigned to either EGFR or cetuximab. Molecules with emission peaks between 650–680 nm (AF647 green window) were assigned to EGFR (or functional antibodies) and molecules with emission peaks between 680–720 nm (CF680 orange window) to total cetuximab antibodies, as illustrated in Fig. 2D. The spectral separation that can be achieved in this particular instrument, which is important for quantitative multiplexing, depends on the spectral precision (σ) of the two fluorophores, which was calculated to be 4 nm for the AF647 and 5.5 $\pm$ 0.5 for the CF680 (ESI Fig. S2†). This allowed for successful 2-color multiplexing quantification since the emission peaks for AF647 and CF680 were sufficiently separated. On average, it was found that the functional Fab fraction was 3.5 times lower than the total amount of cetuximab. Since every antibody has 2 functional flabs, it can be estimated that only 15% fab are accessible to recognize EGFR.

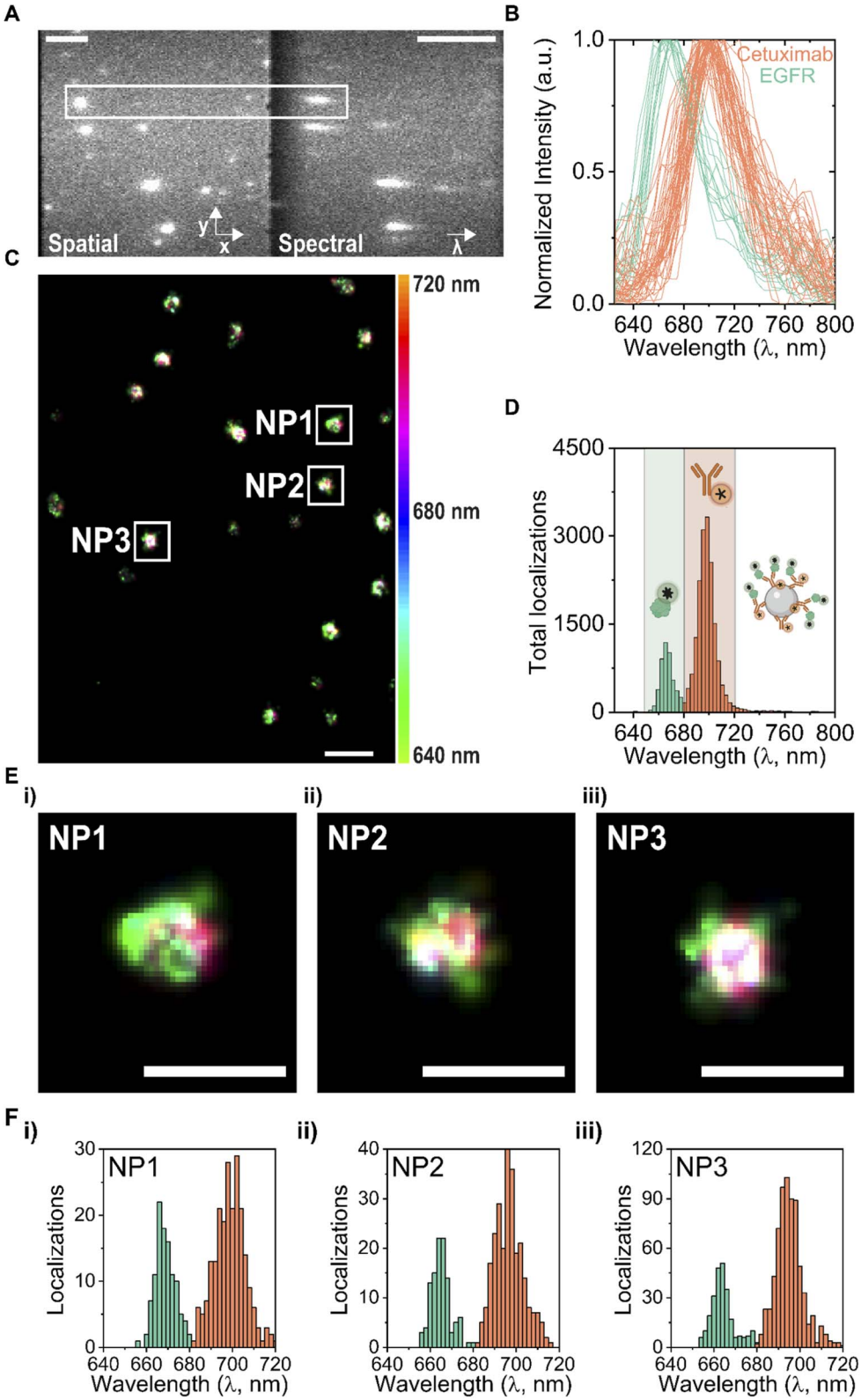

Fig. 2 SR-dSTORM microscopy and quantification on silica NPs functionalized with CF680-labelled cetuximab antibodies and labelled with EGFR-AF647. (A) Single frame of spatial and spectral field of view of the raw data obtained from SR-dSTORM imaging. All the localizations of the individual dSTORM fluorophores in the spatial region carry wavelength information in the spectral region (inset). Scale bars are 2 μm (spatial) and 200 nm (spectral). (B) Single-molecule fluorescence spectrum of all individual blinkings of a selected nanoparticle, where each color denotes either EGFR-AF647 (green) or cetuximab-CF680 (orange) with a peak-to-peak separation of 30 nm. (C) Multiplexing dSTORM reconstruction of functionalized silica NPs (scale bar, 1 μm). (D) Histograms representing the peak wavelength windows (green or orange) of the total dSTORM localizations (AF647 or CF680) in the field of view. (E(i–iii)) Magnified insets of three individual NPs in (C). Scale bar 500 nm. (F) Respective peak wavelength histograms of NPs shown in (E).

Furthermore, an interparticle heterogeneity can be resolved in terms of total and functional amount of antibodies. Fig. 2E and F show a zoom-in of 3 different NPs from the same field of view with their corresponding histograms indicating the amount of localizations per fluorophore detected at a single-particle level. Notably, the relationship between total and functional antibodies can vary substantially at a single-particle level as shown in Fig. 2E and F, giving rise to heterogeneities between NP properties from the same batch. Using quantitative SR-dSTORM analysis, it was possible to assess the heterogeneity of NPs within the same batch.

Before moving to the dSTORM quantification, it is important to introduce a single-particle metric: the functionality ratio, which refers to the ratio between functional and total cetuximab Fab fragments per NP. A systematical screening of different NP formulations was performed to identify if the functionality ratio was constant over different conditions. For this experiment, the amount of cetuximab was varied during the conjugation reaction in the range of 50 to 400 cetuximab per NP, as estimated theoretically. SR-dSTORM localizations needed to be translated into amount of molecules to obtain information about the functionality ratio. For this purpose, a calibration of fluorescent cetuximab and EGFR was performed as previously described (ESI Fig. S3†).[11,21] SR-dSTORM localizations are proportional to the number of molecules on the NP, thus knowing how many localizations correspond to a single cetuximab or EGFR molecule during the imaging acquisition allows for the identification of the amount of functional and total cetuximab antibodies per NP. Finally, the total amount of Fab fragments per NP was

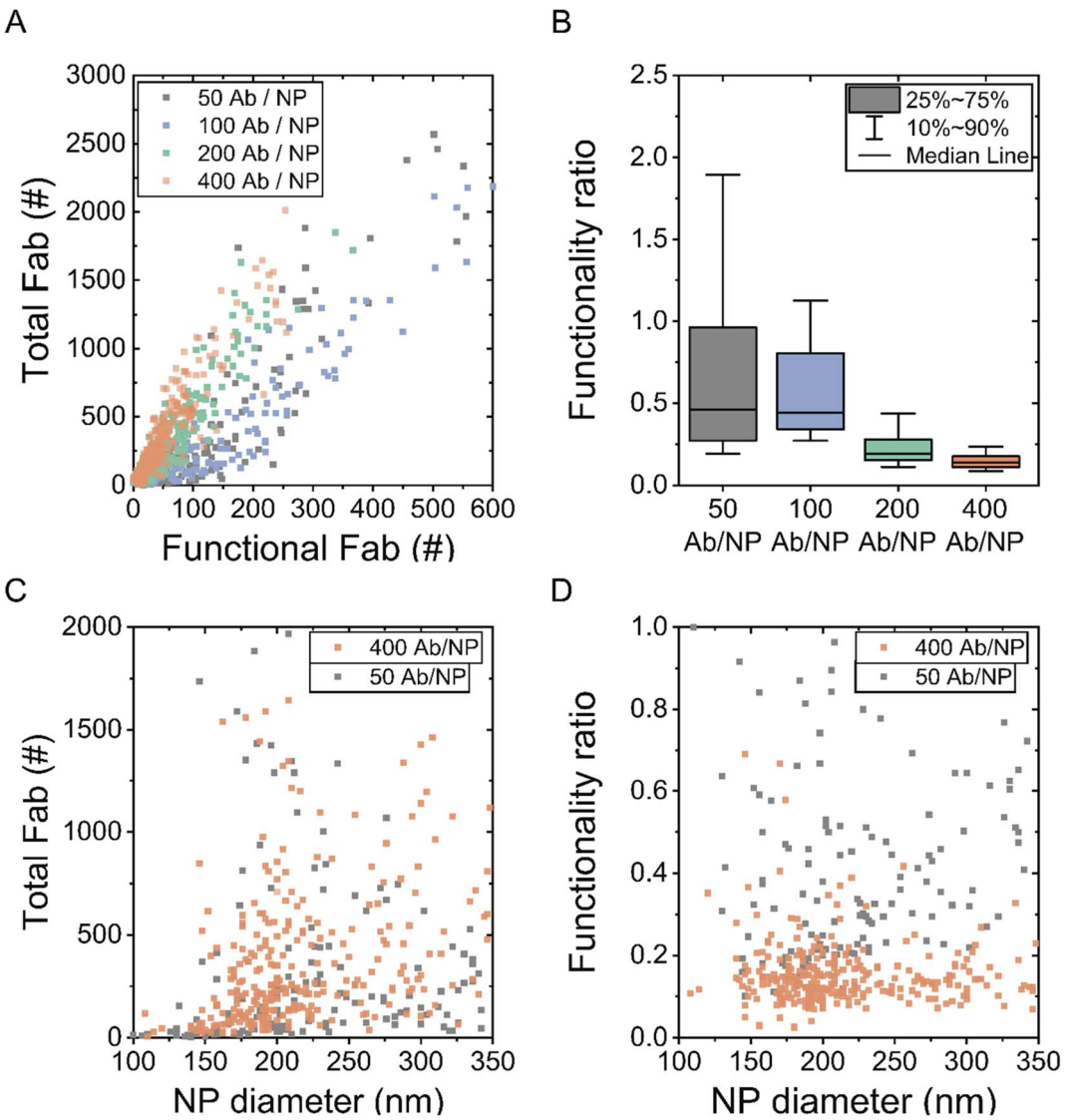

Fig. 3 Quantification of total and functional cetuximab for NP formulations with different amount of total added antibody during chemical conjugation determined by SR-dSTORM. (A) Scatter plot representing functional *versus* total Fab cetuximab fragments available. Each square represents one single NP. Axis are shortened for representation convenience. (B) Box plot representing the functionality ratio (functional divided by total cetuximab Fab) per NP formulation. Box represents the 25% to 75% percentile and whiskers 10% to 90%. Per condition, minimum $N = 100$ NPs were analyzed. (C) Scatter plot representing total Fab *versus* NP diameter. (D) Scatter plot representing functionality ratio *versus* NP diameter.

calculated by multiplying the number of total cetuximab obtained by factor 2.

Fig. 3A displays a scatter plot of functional *versus* total amount of Fab fragments for different NP formulations with an increasing amount of cetuximab during the conjugation. Note that each square represents the properties of a single NP, giving unprecedented insights into the total and functional antibodies at the single-particle level. Qualitatively, each studied formulation seemed to follow a linear trend, with particles having more functionality with increased total amount of conjugated cetuximab. The slope of the line represents the functional ratio where a slope of 1 would correspond to 100% functionality. Interestingly, the trends of the different formulations showed that the more cetuximab added to the formulation (400 antibodies/NP), the less functionality was present, as shown from the subtle shifts of the total Fab-functional Fab slope. This trend was confirmed when looking at the functionality ratio at the single-particle level (Fig. 3B). It was observed that while the functionality ratio median is around 0.5 for low antibody conjugation (50 antibodies/NP), it decreased to 0.2 for higher antibody conjugation conditions (400 antibodies/NP). Note that some NPs presented unrealistic functionality ratios (>1), which could be caused by the experimental variability of STORM microscopy. The unspecific binding properties of EGFR to silica NPs were described in earlier studies,[11] where minimal binding was demonstrated towards bare NPs in the presence of a mild bovine serum albumin (BSA) blocking (protocol in Materials and methods). Finally, Fig. 3C and D illustrate the correlation between total cetuximab Fab or the functionality ratio with the NP diameter, respectively. These results depict that NP size dispersion had little influence on the chemical conjugation method (NP functionalization amounts and functionality), as seen from the single-particle quantification.

Carbodiimide-based conjugation strategies are non-oriented and stochastic, since the carboxylic acid groups from the silica NP can react with any of the exposed primary amines of the cetuximab antibody. Thus, it is expected that not all cetuximab antibodies will be functional to recognize the target. In accordance with a previous estimation reporting only 30% of functional Fabs, it was confirmed experimentally that indeed not all conjugated antibodies are functional to recognize their target.[11] Here, the single-molecule and single-particle quantification depicts that the experimental functionality percentage lies in a similar range (between 20–50% functionality). Furthermore, the results indicate that the functionality ratio also depends on the antibody conjugation concentration. The studied antibody conjugation concentrations are theoretically far from NP surface saturation (estimated at 1328 antibodies/NP for 100 nm radius NPs[11]). The strong dependence of concentration and functionality ratio could thus indicate that higher antibody concentrations result in a higher chance of steric hindrance effects.

In a future outlook, the presented functionality mapping technique can be used to optimize current NP ligand conjugation or can be combined with a multiparametric imaging approach using environmental sensing probes, that change their emission spectrum according to the local nanoenvironment. Specifically, the comparison between non-oriented and oriented conjugation approaches to for maximizing the selectivity towards the target cell and minimizing the adverse effects such as premature immune system clearance due to unfavorable oriented ligands. Additionally, the presented workflow can be relevant in analytical applications, were the functionality of antibodies is imperative for analyte detection and assay sensitivity.[22,23] This includes the single-molecule characterization of antibody-coated particles as well as antibody-coated flat surfaces that are developed for biosensing applications.

In summary, SR-dSTORM characterization of ligand-functionalized NPs is a promising tool to obtain a better understanding into the single-particle functionality properties. In this exploratory work the interplay between NP ligand conjugation and actual NP functionality is illustrated.

Conclusion

Antibody functionality can be compromised after conjugation to a NP surface, but limited information is known about the functional fraction of conjugated antibodies compared to the total conjugated amount. A reduced ligand functionality in addition to adverse effects from antibody orientation minimizes the chances of selective drug delivery to the target site. In this work, SR-dSTORM fluorescence microscopy enabled the simultaneous quantification of total and functional cetuximab antibodies covalently conjugated to silica NPs. The multiplexing capabilities of SR-dSTORM enabled multicolor imaging of fluorophores located in the same emission window providing a single-particle functionality control with single-molecule sensitivity. It was observed that there are substantial interparticle heterogeneities within the same batch. Furthermore, the amount of cetuximab conjugated to NPs was systematically varied and investigated with SR-dSTORM, revealing that different cetuximab concentrations lead to a different ratio between functional and total antibodies. An interesting outlook of the presented approach is the multiparametric imaging of NPs, including NP ligand functionality and other characteristics such as polarity that can be mapped using environmentally-responsive probes. Overall SR-STORM paves the way for further investigation of NP functionality, with the ultimate goal of rationally designing nanomedicines for selective and efficient targeting of the cell of interest.

Materials and methods

Materials

Fluorescent silica NPs (Sicastar®-GreenF) with surface carboxylic acid groups (COOH) of 100 nm radius were purchased from Micromod Partikeltechnologie GmbH. Cetuximab antibody (Erbitux, Merck) was kindly provided by Prof. Marteen Merkx (Eindhoven University of Technology). Human EGFR protein (Fc tag, ACROBiosystems EGR-H5252), Zeba™ desalting columns (7 K MWCO), Alexa Fluor™ 647 NHS ester and HEPES buffer (1 M) were purchased from Thermo Fisher Scientific. Phosphate buffered saline (PBS) tablets, 1-ethyl-3-(3-

dimethylaminopropyl)-carbodiimide (EDC), tris(hydroxymethyl)-amino-methane (tris base), bovine serum albumin (96% purity), cysteamine, catalase from bovine liver, glucose oxidase, sodium bicarbonate and 4-morpholineethanesulfonic acid (MES) were purchased from Merck Life Science. CF®680 NHS ester was obtained from VWR International BV.

Fluorescent labeling of cetuximab and EGFR

Before labeling with a fluorescent dye, cetuximab solution was buffer exchanged to sodium bicarbonate (pH 8.4 0.1 M) using a Zeba™ desalting column. Cetuximab was incubated with CF®680 NHS ester and EGFR was incubated with Alexa Fluor™ 647 NHS ester both at a 1 : 6 protein : dye mol ratio for 2 h at 22 °C and 400 rpm in a ThermoMixer® (Eppendorf). The reaction mixtures were purified using 2 consecutive Zeba™ desalting columns rinsed with PBS buffer according to the manufacturer's protocol. The labelled proteins were measured with a NanoDrop™ One (Thermo) to calculate their respective degree of labeling (PBS was used as a blank in both cases), yielding 3 : 3 dye : protein mol ratios for both cetuximab-CF680 and EGFR-AF647.

Synthesis of cetuximab-conjugated silica NPs

Cetuximab-CF680 was chemically conjugated to silica NPs with surface carboxylic acid groups *via* 1-ethyl-3-(3-dimethylaminopropyl)-carbodiimide (EDC) coupling chemistry. First, NPs were diluted in 500 μl MES buffer (50 mM, pH 5) and centrifuged for 10 minutes at 16 000 to remove the NP storage solution. NPs were resuspended in MES buffer (50 mM, pH 5) containing 2 mM EDC to activate the carboxylic acid NP groups and incubated for 15 minutes at 22 °C and 400 rpm in a ThermoMixer®. Next, NPs were sonicated for 5 minutes in a bath sonicator and cetuximab-CF680 was added to the activated NPs at the appropriate concentration and incubated for 2 h at 22 °C and 400 rpm in a ThermoMixer®. Specifically, cetuximab-CF680 was added at 50, 100, 200 and 400 antibody/NP calculated from theoretical estimations. Unconjugated cetuximab-CF680 was purified by centrifuging thrice at 16000 g for 15 minutes and washing with 25 mM HEPES buffer. Silica-cetuximab680 NPs were resuspended at a final concentration of 2 mg ml^{-1} in 25 mM HEPES buffer and stored at 4 °C.

Sample preparation for SR-dSTORM microscopy

Before SR-dSTORM imaging silica-cetuximab680 NPs were incubated with the EGFR-AF647 probe to label the cetuximab functional sites. Therefore, 25 μg of silica-cetuximab680 NPs were mixed with 20 pmol EGFR-AF647 probe, 0.5% BSA to block the unspecific binding and HEPES (25 mM) buffer to make up to 40 μl of total volume and incubated for 1 h at 25 °C and 400 rpm in a ThermoMixer®. NPs were sonicated in a bath sonicator for 5 minutes and imaged the same day. To image NPs, we created a microscopy imaging chamber consisting of one coverslip attached to a microscope slide using double-sided scotch tape (approximate volume of the chamber was 20 μl). For that, coverslips (22 × 22 mm, #1.5) were sonicated in isopropanol for 20 minutes and dried under nitrogen flow, and microscope slides (76 × 26 mm, thickness 1 mm) were cleaned using an isopropanol-soaked tissue before each experiment. Silica-cetuximab680 labelled with EGFR-AF647 NPs were incubated in the imaging chamber and allowed to adsorb between 30–60 minutes at room temperature. After NP attachment, the imaging chamber was rinsed once with 200 μl HEPES buffer (25 mM) to remove non-attached NPs and subsequently rinsed with 100 μl STORM buffer[24] (50 mM tris pH 8, 10 mM NaCl, 10% w/v glucose, 50 mM cysteamine, 0.5 mg ml^{-1} glucose oxidase, 40 μg ml^{-1} catalase). The imaging chamber was then sealed with nail polish and imaged immediately.

Optical instrumentation

AF647 and CF680 fluorophores were excited with a 100 mW, 637 nm continuous fiber-coupled wavelength source (OBIS FP 637LX, Coherent OBIS). The excitation beam was directed through a dichroic mirror (ZT640rdc, Chroma) to an oil-immersion objective lens (Nikon Apo TIRF 100× Oil DIC N2). The fluorescence was further directed off a notch filter (ZET635NF, Chroma), a long-pass filter, a mechanical slit (VA100C, Thorlabs) and a diffraction grating (70 grooves per mm, 25 × 25 mm-46-068, Edmund) to an EMCCD camera (Andor DU-888 X-9414). The electron multiplication gain was 250, exposure time 30 ms and pixel size 90 nm.

Spectral precision (σ)

First, the spectral displacement of the localizations was calculated for (i) NPs which consisted of only CF680-labelled cetuximab and (ii) NPs which consisted of only AF647-labelled EGFR. Afterwards, by fitting the displacements with a Gaussian profile, the mean spectral displacement for every NP was calculated. Finally by binning and fitting all single-particle mean displacements the final spectral precision was calculated for either the CF680 or AF647 nanoparticles by fitting with a Gaussian profile (ESI Fig. S2†).

SR-dSTORM quantification

The localization files which contain the single-molecule coordinates (X, Y, T) and the raw single-molecule fluorescence spectrum of AF647 and CF680 were obtained *via* ThunderSTORM and RainbowSTORM for Fiji.[25,26] Additionally, the first 1500 frames were filtered out to wait for the proper STORM blinking to occur. Furthermore, a density filter (radius 80 nm, neighbors 80) was applied to filter out the nonspecific localizations which occur like sparse points in the field of view. Then, a Gaussian profile was used to calculate the emission peak values from each single-molecule spectrum in the localization file and each localization was assigned to either AF647 (which corresponds to EGFR) or CF680 (which corresponds to cetuximab) fluorophore. The assignment was made based on two wavelength windows: 650 nm to 680 nm assigns the localization to EGFR while 681 nm to 720 nm assigns the localization to cetuximab. The amount of localizations in each window denotes the amount of either EGFR probes or total cetuximab antibodies and fab fragments. Finally, all NPs with their localizations were grouped (bandwidth 150 nm, minimum number

of localizations 20) and filtered based on their size and elongation using a mean-shift clustering script (MATLAB) which was previously described.[11] To correlate the number of localizations with the number of cetuximab-CF680 or EGFR-AF647 molecules, a calibration was performed as previously described[11,21] to estimate the number of localizations obtained per single-molecule under the same imaging conditions at a very low protein concentration (0.1 nM and 3.5 nM, respectively) attached to a cover glass (ESI Fig. S3†). The calibration yielded 1.3 localizations per cetuximab-CF680 and 1.2 localizations per EGFR-AF647 molecule.

SR-dSTORM multiplexing reconstructions

After peak fitting the spectrum of all single-molecule localizations, the localization file was updated and imported into the RainbowSTORM plugin for visualization either using scatter plot or average histograms.

Conflicts of interest

There are no conflicts to declare.

Acknowledgements

This project has received funding from the European Union's Horizon 2020 research and innovation program under the Marie Skłodowska-Curie [grant agreement no. 765497 (THERACAT)]. This work was financially supported by the European Research Council (ERCStG-757397).

References

1 M. J. Mitchell, M. M. Billingsley, R. M. Haley, M. E. Wechsler, N. A. Peppas and R. Langer, *Nat. Rev. Drug Discovery*, 2021, **20**, 101–124.
2 A. M. Alkilany, L. Zhu, H. Weller, A. Mews, W. J. Parak, M. Barz and N. Feliu, *Adv. Drug Delivery Rev.*, 2019, **143**, 22–36.
3 J.-B. Coty and C. Vauthier, *J. Controlled Release*, 2018, **275**, 254–268.
4 M. C. Johnston and C. J. Scott, *Drug Discovery Today: Technol.*, 2018, **30**, 63–69.
5 I. Van Zundert, M. Bravo, O. Deschaume, P. Cybulski, C. Bartic, J. Hofkens, H. Uji-i, B. Fortuni and S. Rocha, *Pharmaceutics*, 2021, **13**, 2153.
6 C. Kappel, C. Seidl, C. Medina-Montano, M. Schinnerer, I. Alberg, C. Leps, J. Sohl, A.-K. Hartmann, M. Fichter, M. Kuske, J. Schunke, G. Kuhn, I. Tubbe, D. Paßlick, D. Hobernik, R. Bent, K. Haas, E. Montermann, K. Walzer, M. Diken, M. Schmidt, R. Zentel, L. Nuhn, H. Schild, S. Tenzer, V. Mailänder, M. Barz, M. Bros and S. Grabbe, *ACS Nano*, 2021, **15**(9), 15191–15209.
7 A. C. Marques, P. J. Costa, S. Velho and M. H. Amaral, *J. Controlled Release*, 2020, **320**, 180–200.
8 L. Woythe, N. B. Tito and L. Albertazzi, *Adv. Drug Delivery Rev.*, 2021, **169**, 1–21.
9 J.-M. Rabanel, V. Adibnia, S. F. Tehrani, S. Sanche, P. Hildgen, X. Banquy and C. Ramassamy, *Nanoscale*, 2019, **11**, 383–406.
10 T. Andrian, P. Delcanale, S. Pujals and L. Albertazzi, *Nano Lett.*, 2021, **21**(12), 5360–5368.
11 L. Woythe, P. Madhikar, N. Feiner-Gracia, C. Storm and L. Albertazzi, *ACS Nano*, 2022, **16**, 3785–3796.
12 L. M. Herda, D. R. Hristov, M. C. Lo Giudice, E. Polo and K. A. Dawson, *J. Am. Chem. Soc.*, 2017, **139**, 111–114.
13 A. Fleming, L. Cursi, J. A. Behan, Y. Yan, Z. Xie, L. Adumeau and K. A. Dawson, *Bioconjugate Chem.*, 2022, **33**(3), 429–443.
14 S. Pujals and L. Albertazzi, *ACS Nano*, 2019, **13**, 9707–9712.
15 Y. Zhang, K.-H. Song, B. Dong, J. L. Davis, G. Shao, C. Sun and H. F. Zhang, *Appl. Opt.*, 2019, **58**, 2248–2255.
16 M. N. Bongiovanni, J. Godet, M. H. Horrocks, L. Tosatto, A. R. Carr, D. C. Wirthensohn, R. T. Ranasinghe, J.-E. Lee, A. Ponjavic, J. V. Fritz, C. M. Dobson, D. Klenerman and S. F. Lee, *Nat. Commun.*, 2016, **7**, 13544.
17 J.-E. Lee, J. C. Sang, M. Rodrigues, A. R. Carr, M. H. Horrocks, S. De, M. N. Bongiovanni, P. Flagmeier, C. M. Dobson, D. J. Wales, S. F. Lee and D. Klenerman, *Nano Lett.*, 2018, **18**, 7494–7501.
18 S. Moon, R. Yan, S. J. Kenny, Y. Shyu, L. Xiang, W. Li and K. Xu, *J. Am. Chem. Soc.*, 2017, **139**, 10944–10947.
19 R. Yan, S. Moon, S. J. Kenny and K. Xu, *Acc. Chem. Res.*, 2018, **51**, 697–705.
20 B. Dong, L. Almassalha, B. E. Urban, T.-Q. Nguyen, S. Khuon, T.-L. Chew, V. Backman, C. Sun and H. F. Zhang, *Nat. Commun.*, 2016, **7**, 12290.
21 N. Feiner-Gracia, M. Beck, S. Pujals, S. Tosi, T. Mandal, C. Buske, M. Linden and L. Albertazzi, *Small*, 2017, **13**, 1701631.
22 B. Saha, P. Songe, T. H. Evers and M. W. J. Prins, *Analyst*, 2017, **142**, 4247–4256.
23 A. K. Trilling, J. Beekwilder and H. Zuilhof, *Analyst*, 2013, **138**, 1619.
24 A. Jimenez, K. Friedl and C. Leterrier, *Methods*, 2020, **174**, 100–114.
25 M. Ovesný, P. Křížek, J. Borkovec, Z. Švindrych and G. M. Hagen, *Bioinformatics*, 2014, **30**, 2389–2390.
26 J. L. Davis, B. Soetikno, K.-H. Song, Y. Zhang, C. Sun and H. F. Zhang, *Bioinformatics*, 2020, **36**, 4972–4974.